Available online at www.sciencedirect.com
SCIENCE DIRECT®
International Journal of Machine Tools & Manufacture 45 (2005) 21–28
INTERNATIONAL JOURNAL OF MACHINE TOOLS & MANUFACTURE DESIGN, RESEARCH AND APPLICATION
www.elsevier.com/locate/ijmactool

Modelling of the mist formation in a segmented grinding wheel system

T. Nguyen, L.C. Zhang *

School of Aerospace, Mechanical and Mechatronic Engineering, The University of Sydney, Sydney, NSW 2006, Australia

Received 28 April 2004; accepted 29 June 2004

Abstract

It has been found that using a segmented grinding wheel with a fluid chamber can significantly minimise the quantity of coolant while improving the ground surface integrity. The present investigation aims to explore the fluid flow mechanism in such a wheel system. To this end, the Weber theory for Newtonian jet instability was applied to quantitatively determine the contribution of coolant flow rate to mist and ligament modes. A semi-analytical model was then developed to predict the mist flow rate by taking into account both the grinding parameters and fluid properties. It was shown that the model prediction was in good agreement with experimental measurements. Because of the comprehensive integration of variables in the formulation, the model provides a good fundamental understanding of the mist formation and offers a practical guideline for the selection and use coolant in minimising the mist flow rate.
© 2004 Elsevier Ltd. All rights reserved.

Keywords: Segmented grinding wheel; Coolant chamber; Mist formation; Grinding coolant optimisation

1. Introduction

Thermal damage is one of the major process limitations in grinding where a workpiece experiences heating within a small grinding zone. Therefore, rapid convective heat dissipation within the zone is essential. However, the convection capacity depends largely on the quantity of coolant that penetrates into the zone [1]. On the other hand, since grinding nowadays is often operated at high spindle speeds, spinning-off of coolant and evaporation caused by high temperature [2] have posed a considerable problem in maintaining the cooling layer at the wheel–work interface.

Suto et al. [3] introduced a segmented grinding wheel structured with perforated holes to allow coolant to impinge radially onto the working surface. This type of wheels was used to grind difficult-to-machine materials at creep feed mode where the fluid was introduced to the grinding zone by centrifugal forces. It was reported that such wheels could bring a significant reduction of specific energy of about 36%. The present authors made a further development by attaching a pressurised fluid chamber to enforce the coolant to penetrate into the grinding zone [4]. In this way, the surface quality of workpieces was improved with only 30% of coolant used in a conventional system. Adhesion of ground chips on the wheel surface disappeared and surface tensile residual stresses caused by thermal deformation were eliminated. This technique has led to a clear enhancement of coolant transportation to improve the heat removal in grinding, but no investigation has been conducted to rationalise the control of coolant application. In the new grinding system, coolant is injected through the small holes on the rotating wheel. In this case, high speed liquid jets are more susceptibly disintegrated into drops because of the interfacial instability of the jets [5]. Furthermore, the exposure of liquid jets to ambient will cause distortion of the flow field. An improper setting of grinding parameters, such as wheel speed and coolant pressure, can significantly reduce the coolant penetration into the grinding zone and generates mist to cause environmental hazards.

* Corresponding author. Tel.: +61-2-9351-2835; fax: +61-2-9351-7060.
E-mail address: zhang@aeromech.usyd.edu.au (L.C. Zhang).

0890-6955/$ - see front matter © 2004 Elsevier Ltd. All rights reserved.
doi:10.1016/j.ijmachtools.2004.06.019

Nomenclature

a, b, c, d	correlation power factors, Eq. (14)
A_1	cross-sectional area of the fluid chamber defined in Eq. (5), m^2
A_2	total cross-sectional area of perforated holes in contact with the fluid chamber, defined in Eq. (5), m^2
C_f	fluid chamber design coefficient defined in Eq. (7), m^{-4}
C_c	dimensionless correlation coefficient, Eq. (14)
d_l	mean diameter of a ligament, m
d_n	diameter of a perforated hole, m
f_c	centrifugal force exerting on a unit volume of coolant, N m^{-3}
l	break-up length of a ligament, m
N	number of liquid jets
n	number of perforated holes in contact with the fluid chamber, Eq. (6)
p_1, p_2	pressure of coolant at planes 1 and 2 in Fig. 4, respectively, Pa
$\bar{p}$	mean pressure of surrounding resistance to the wheel rotation, Pa
$\bar{p}_n$	mean transverse pressure exerting on a ligament, Pa
Q	total flow rate of supplied coolant, $m^3\ s^{-1}$
Q_{li}	flow rate of a ligament, $m^3\ s^{-1}$
Q_l	total flow rate contributed to ligaments, $m^3\ s^{-1}$
Q_m	flow rate contributed to mist formation, $m^3\ s^{-1}$
Q_m^*	mist flow rate ratio
R	radius of the grinding wheel, m
Re	Reynolds number, Eq. (19) ($Re = \rho v_l d_l/\mu$)
Re^*	Reynolds number, Eq. (13) ($Re^* = \rho\omega R^2/\mu$)
Re_c	critical Reynolds number, Eq. (20)
v_l	velocity of a ligament, m s^{-1}
$\bar{V}_1, \bar{V}_2$	mean velocity of coolant flowing through planes 1 and 2 in Fig. 4, respectively, m s^{-1}
Oh	Ohnesorge number, Eq. (18) ($Oh = \mu/(\rho\sigma d)^{0.5}$)
We	Weber number, Eq. (16) ($We = \rho d_l v_l^2/\sigma$)
We^*	Weber number, Eq. (13) ($We^* = \rho\omega^2 R^3/\sigma$)
Δp	static pressure drop through the perforated holes, Pa
Δp^*	pressure influence number
Y	dimensionless grinding variable, defined in Eq. (14)
δ	disturbance amplitude, Eq. (16), m
ρ	coolant density, kg m^{-3}
σ	surface tension of coolant, N m^{-1}
μ	dynamic viscosity of coolant, N s m^{-2}
ϕ	alignment angle of the coolant chamber defined in Fig. 2, rad
ϕ^*	transverse flow influence number, Eq. (13)
φ	distortion angle of a ligament defined in Fig. 5, rad
ω	rotational grinding wheel speed, rad s^{-1}

This paper aims to understand the mechanism of coolant disintegration and to facilitate the optimisation of the parameter setting using the segmented wheel/fluid chamber system.

2. Experimental apparatus

Fig. 1 shows the structure of a grinding wheel with a fluid chamber [4] whose position can be adjusted with an angle ϕ relative to the vertical axis of the grinding wheel (Fig. 2). The experimental parameters are listed in Table 1.

Instantaneous images of the fluid flow during high-speed rotation of the wheel were recorded by high-speed strobe photography, where a stroboscope (1538-A Strobotac) with its flash duration less than 3 μs was used in synchronisation with a camera (Nikon 35-135). The obtained images were analysed by a programme, Leica Qwin, which was installed in a microscope system, Leica DMRXE. The coolant vis-

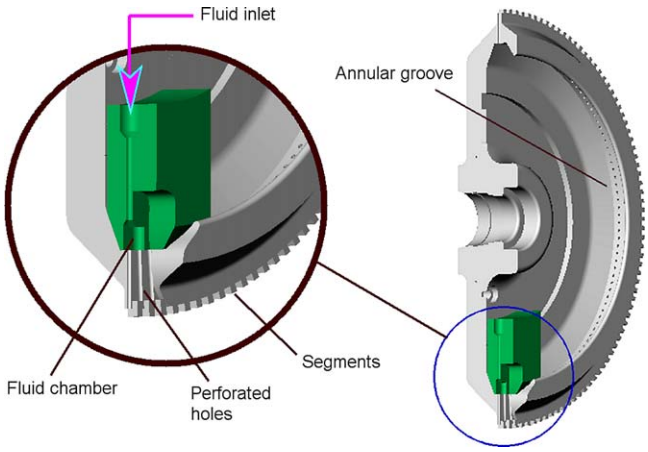

Fig. 1. Section view of the segmented wheel/fluid chamber system.

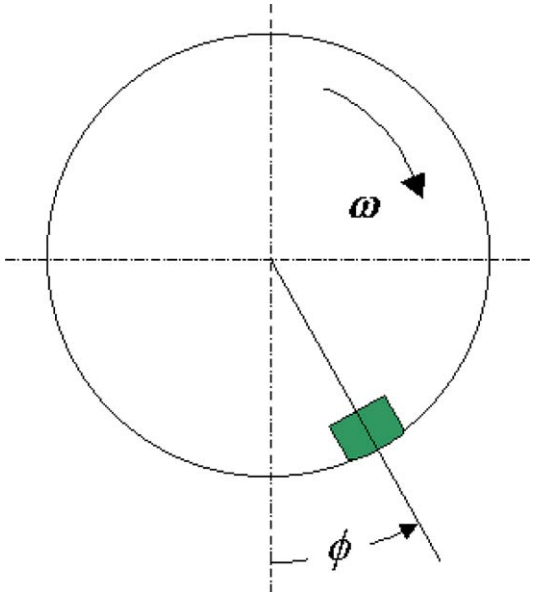

Fig. 2. Alignment of the coolant chamber.

cosity was measured using a Stress Tech. Reologica Instrument machine.

3. Modelling

3.1. Understanding of mist formation

3.1.1. Flow rate and ligament instability

Fig. 3 illustrates some typical flow fields of coolant injected through the perforated holes of the grinding wheel. The flow consists of several liquid jets formed in ligament mode. The total flow rate through the system Q, can be expressed by the equation of mass conservation:

$$Q = Q_m + Q_l = Q_m + \sum_{i=1}^{N} Q_{li} \quad (1)$$

where Q_m and Q_l, respectively, are the flow rate contributed to mist formation and ligament mode, Q_{li} is the flow rate of an individual ligament and N is the number of ligaments.

According to Lefebvre [6], the disintegration of bulk liquid into small drops is caused by the loss of stability during the development of waves on the liquid surface. When a liquid jet emerges from a nozzle as a continuous body, there is a competition set up on the surface of the jet between the cohesive and disruptive forces, giving rise to oscillations and perturbations. Surface tension is active as a cohesion that restrains the liquid without breaking up into drops. In contrast, aerodynamic forces acting on the liquid surface promote disruptions. Break-up occurs when the magnitude of the disruptive forces exceeds the surface tension. The role of viscosity, on the other hand, is to inhibit the growth of instabilities and generally delays the onset of disintegration [7–10].

The above understanding shows that the disruptions of coolant jets are of internal and external origins and can be analysed by superposing the internal disturbances and external interaction with the surrounding media. As clearly demonstrated in Fig. 3, the disturbances are due to (i) the wheel rotation ω, (ii) the static pressure drop of liquid through the perforated holes caused by the geometric details of the fluid chamber Δp, and (iii) the alignment, ϕ, of the fluid chamber in the system. These causes are discussed below.

3.1.2. Wheel speed

The disintegration of liquid jets is influenced by wheel speed in two aspects. Firstly, it depends on the magnitude of the centrifugal force caused by the wheel rotation, i.e.

$$f_c = \rho R \omega^2 \quad (2)$$

where f_c is the centrifugal force exerting on a unit volume of coolant, ρ is the coolant density, R and ω are the radius and rotational speed of the wheel, respectively.

Secondly, it depends on the interaction of the liquid jets with the surrounding media. For instance, an increase in air velocity will accelerate the jet break-up [9]. In the present application, coolant jets are influenced by two motions, the radial motion caused by the developed pressure in the fluid chamber and the rotation of the grinding wheel which lead to "slippage" between the liquid and the wheel and make the liquid jets point to the direction of the wheel rotation, as shown in Fig. 3. As a result, an increase of the wheel speed will increase the aerodynamic destabilising effect on the jets surface, thus rasing the disintegration of coolant jets into mist.

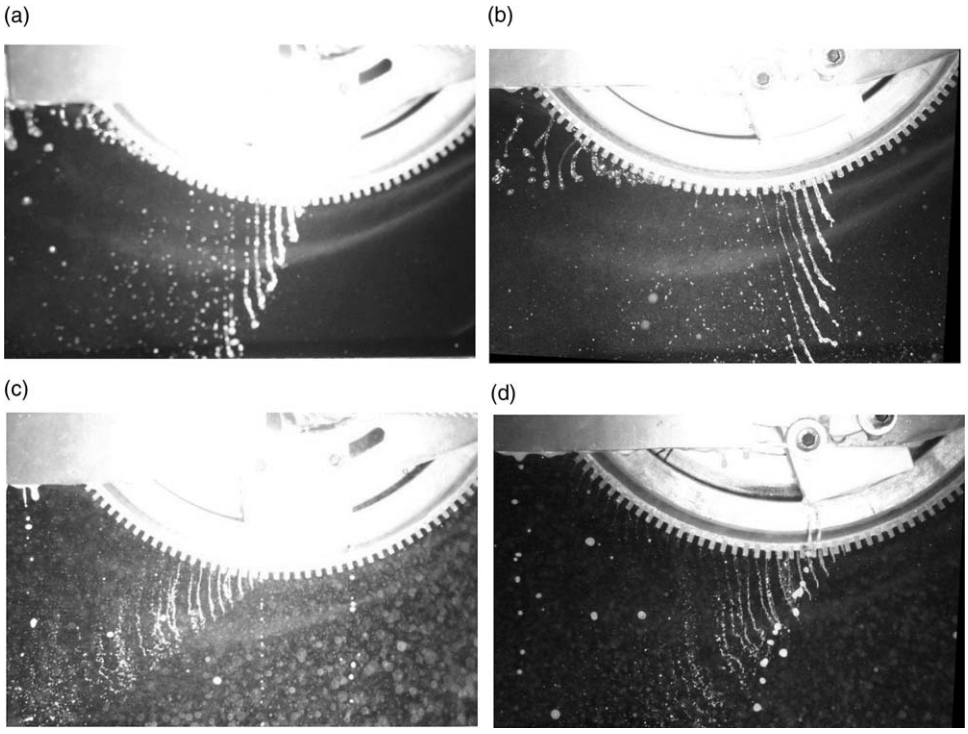

Fig. 3. Coolant flows at $Q = 4.8\ \mathrm{l\ min^{-1}}$: (a) $\omega = 100$ rpm and $\phi = 0^{\circ}$; (b) $\omega = 100$ rpm and $\phi = 30^{\circ}$; (c) $\omega = 1000$ rpm and $\phi = 0^{\circ}$; and (d) $\omega = 1000$ rpm and $\phi = 30^{\circ}$.

3.1.3. Static pressure drop

High pressure drop will increase the discharged velocity of the coolant jets and promotes their disintegration into fine mists [5,6]. The magnitude of the static pressure drop between the fluid chamber and ambient, Δp, can be determined using the Bernoulli equation between planes 1 and 2 as shown in Fig. 4:

$$\frac{p_1}{\rho} + \frac{\bar{V}_1^2}{2} + gz_1 = \frac{p_2}{\rho} + \frac{\bar{V}_2^2}{2} + gz_2 \tag{3}$$

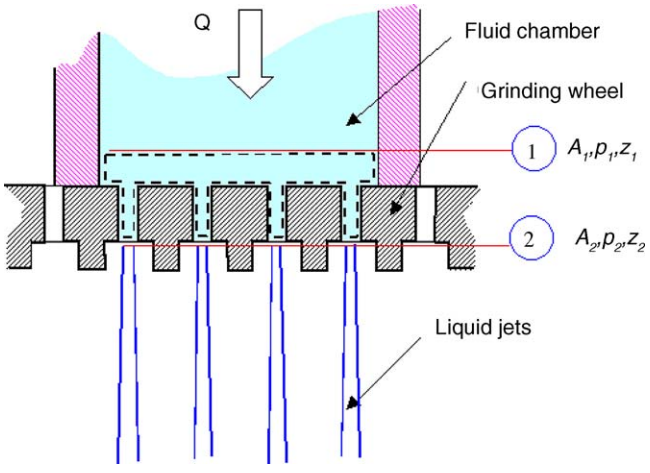

Fig. 4. Schematic of liquid flow from the channel to the holes.

where $\bar{V}_1$ and $\bar{V}_2$ are the mean velocities at planes 1 and 2, respectively. Since the small distance between the two planes ($z_1 - z_2$), Eq. (3) can be approximated as

$$\Delta p = p_1 - p_2 = \rho \frac{\bar{V}_2^2 - \bar{V}_1^2}{2} \tag{4}$$

On the other hand, the continuity equation for a steady incompressible flow gives rise to

$$Q = A_1 \bar{V} = A_2 \bar{V}_2 \tag{5}$$

or $\bar{V}_1 = Q/A_1$ and $\bar{V}_2 = Q/A_2$ where A_1 is the cross-sectional area of the fluid chamber and A_2 is the total cross-sectional area of the perforated holes within the chamber. If the number of the perforated holes within the chamber is n and the diameter of each hole is d_n, A_2 is derived as

$$A_2 = n \frac{\pi d_n^2}{4} \tag{6}$$

Then, Eqs. (4) and (5) give rise to

$$\Delta p = \frac{Q^2 \rho}{2} \left(\frac{A_1^2 - A_2^2}{A_1^2 A_2^2} \right) = C_{\mathrm{f}} \left(\frac{Q^2 \rho}{2} \right) \tag{7}$$

where $C_{\mathrm{f}} = (A_1^2 - A_2^2)/A_1^2 A_2^2$ can be considered as a coefficient representing the influence of the chamber design on Δp.

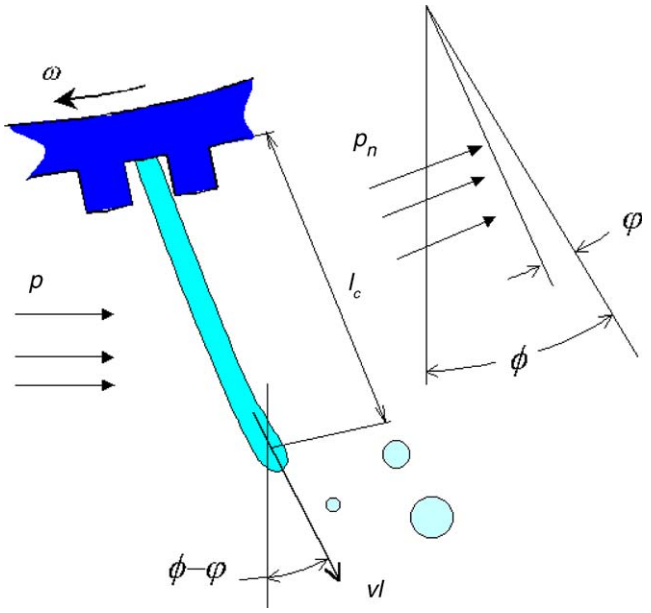

Fig. 5. Parameter definitions of a jet.

3.1.4. Alignment of the fluid chamber

From the sketches shown in Figs. 2 and 4, the transverse effect of the surrounding media on a ligament at a given wheel speed can be expressed as

$$\int_0^l \int_0^{d_l} \bar{p}_n \, \mathrm{d}(d_l)\mathrm{d}l = \int_0^l \int_0^{d_l} \bar{p}|\cos(\phi - \varphi)|\mathrm{d}(d_l)\mathrm{d}l \tag{8}$$

where $\bar{p}_n$ is the mean transverse pressure on a ligament, $\bar{p}$ is the mean pressure developed by the surrounding media resisting the wheel rotation and φ is the distortion angle defined in Fig. 5.

The images in Fig. 3 show that the ligament can be considered to be cylindrical. As a first approximation, the distortion angle φ can be neglected. Eq. (8) therefore becomes

$$\int_0^l \int_0^{d_l} \bar{p}_n \, \mathrm{d}(d_l)\mathrm{d}l = \bar{p}d_l l|\cos\phi| \tag{9}$$

This equation shows that the disruption of a ligament caused by the transverse flow at a given wheel speed depends on the alignment of the fluid chamber, $\cos\phi$.

3.2. Dimensional analysis

Dimensional analysis has been proved to be successful and effective in generating analytical formulae for complex systems involving a large number of variables such as rolling [11,12], polishing [13], grinding [14–16], and metal forming [17]. With the understanding achieved in the above sections, we are now able to develop a parametric model to predict the mist flow rate.

The aforementioned physical understanding indicates that the flow rate contributed to the mist formation, Q_m, can be expressed as

$$Q_\mathrm{m} = f(\rho,\sigma,\mu,\omega,\Delta p,Q,R,\phi,A_1,d_n,n) \tag{10}$$

where density ρ, surface tension σ, and viscosity μ are fluid properties; wheel speed ω, static pressure drop through the coolant chamber Δp, total coolant flow rate Q, wheel diameter R, and alignment angle of the coolant chamber ϕ are grinding parameters; A_1, d_n and n are fluid chamber details defined previously.

From the analysis in previous sections, Eq. (10) can be rearranged as

$$f(C_f,Q_\mathrm{m},Q,\rho R\omega^2,\sigma,\mu,\cos\phi) = 0 \tag{11}$$

The Buckingham Π theorem allows the relationship to be expressed in the form

$$f(\pi_1,\pi_2,\pi_3,\pi_4,\phi^*) = 0 \tag{12}$$

where the non-dimensional variables are

$$\pi_1 = \frac{Q_\mathrm{m}}{Q} = Q_\mathrm{m}^*$$

$$\pi_2 = \frac{\rho\omega R^2}{\mu} = Re^*$$

$$\pi_3 = \frac{\rho\omega^2 R^3}{\sigma} = We^*$$

$$\pi_4 = \frac{C_f Q^2}{2(\omega R)^2} = \frac{\Delta p}{\rho(\omega R)^2} = \Delta p^*$$

$$\phi^* = |\cos\phi|$$

Hence, Eq. (12) can be rewritten as:

$$Q_\mathrm{m}^* = f(Re^*,We^*,\Delta p^*,\phi^*) \tag{13}$$

The physical meanings of the characteristic variables in Eq. (13) are:

- Re^*, the Reynolds number representing the effect of viscosity on the flow at a given wheel speed.
- We^*, the Weber number standing for the ratio between aerodynamic forces acting on ambient gas to surface tension at a given wheel speed.
- Δp^*, the pressure influence number which is the ratio of the work done by pressure drop to kinetic energy, where the pressure drop is caused by forcing the flow through the perforated holes and the kinetic energy is developed by the wheel rotation.
- ϕ^*, the transverse flow influence number representing the transverse effect of aerodynamic forces on destabilisation of liquid jets, caused by the alignment of the fluid chamber in the grinding system.

Although the specific format of function f in Eq. (13) is unknown, according to the principle of dimensional

analysis, it can be approximately expressed as

$$Q_{\mathrm{m}}^{*} = C_{\mathrm{c}} Y \tag{14}$$

where

$$Y = (Re^{*})^{a}(We^{*})^{b}(\Delta p^{*})^{c}(\phi^{*})^{d}$$

3.3. Contribution of flow rate to different modes

The correlation developed above requires the flow rate contributed to mist formation, Q_{m}. As shown in Fig. 3, mist is not evenly dispersed in the surrounding media, but varies in drop size and concentration. Therefore, a direct determination of the mist flow rate is difficult. However, we noticed that the dimensions of liquid ligaments can be accurately obtained from the Leica Qwin image analysis. We therefore use the following method to determine the flow rates contributed to ligament and mist formation.

Assuming that the liquid ligament is cylindrical, the flow rate of individual ligament, $Q_{\mathrm{l}i}$ can be determined as

$$Q_{\mathrm{l}i} = \frac{\pi d_{\mathrm{l}}^{2}}{4} v_{\mathrm{l}} \tag{15}$$

where d_{l} and v_{l} are the diameter and velocity of a ligament, respectively.

According to the Weber theory [5,18] for the instability of Newtonian jets, the break-up length l of a liquid jet subjected to the forces of surface tension and inertia is

$$\frac{l}{d_{\mathrm{l}}} = \ln\left(\frac{d_{\mathrm{l}}}{2\delta}\right) We^{0.5}(1 + 3Oh) \tag{16}$$

where δ is the amplitude of disturbance; We and Oh is the Weber and Ohnesorge number, respectively, defined as

$$We = \frac{\rho d_{\mathrm{l}} v_{\mathrm{l}}^{2}}{\sigma} \tag{17}$$

$$Oh = \frac{\mu}{(\rho\sigma d_{\mathrm{l}})^{0.5}} \tag{18}$$

The parameter $\ln(d_{\mathrm{l}}/2\delta)$ depends on the nature of the jet, i.e. laminar or turbulent, which is determined by the following condition [19]:

$Re < Re_{\mathrm{c}}$: laminar flow

$Re > Re_{\mathrm{c}}$: turbulent flow

where

$$Re = \rho v_{\mathrm{l}} d_{\mathrm{l}} \mu^{-1} \tag{19}$$

and

$$Re_{\mathrm{c}} = 1.2 \times 10^{4}\left(\frac{1}{d}\right)^{-0.3} \tag{20}$$

For a laminar flow, according to Grant et al. [8]:

$$\ln\left(\frac{d_{\mathrm{l}}}{2\delta}\right) = 7.68 - 2.66Oh, \tag{21}$$

but for a turbulent flow, Eq. (2) becomes [8]

$$\frac{l}{d_{\mathrm{l}}} = 8.51 We^{0.32} \tag{22}$$

Now, $Q_{\mathrm{l}i}$ can be determined following the steps shown in Fig. 6.

Due to the light scattering from ruffles on the jet surface produced by random fluctuation of the velocity components, the turbulent jets have "milky" surfaces [5,8]. This is confirmed by the experimental observation shown in Fig. 7.

Finally, the contribution of flow rates due to ligament and mist formation can be determined using Eq. (1).

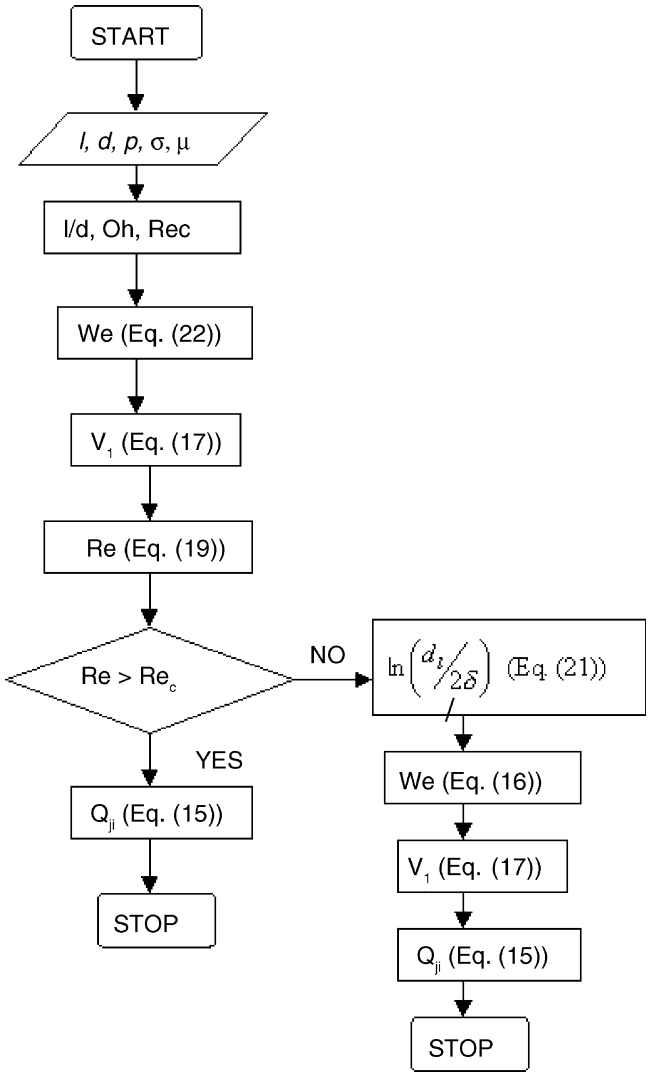

Fig. 6. Steps for determining $Q_{\mathrm{l}i}$.

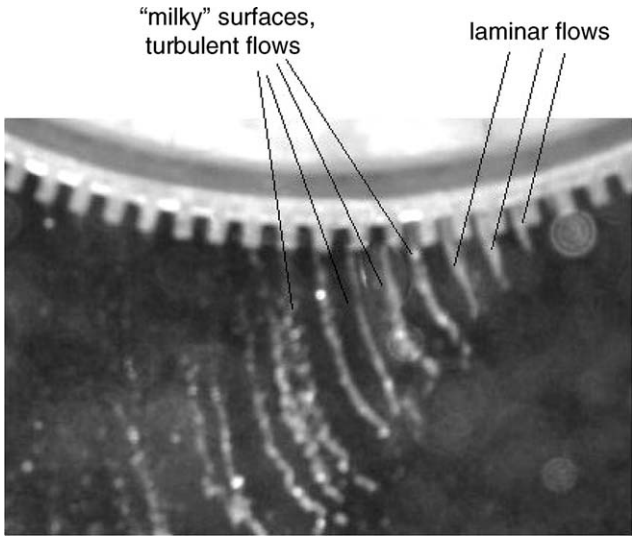

Fig. 7. The "milky" jet surfaces indicating the surface instability of turbulent flow.

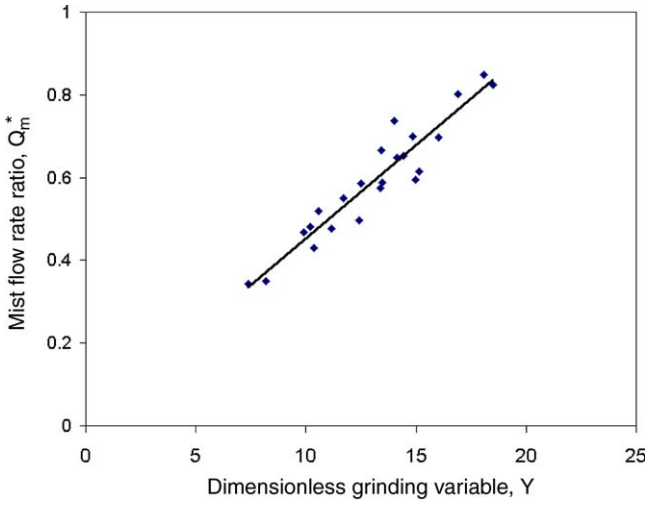

Fig. 8. Comparison of model prediction (solid line) and experimental measurements (dots), where $Y=(Re^*)^a(We^*)^b(\Delta p^*)^c(\phi^*)^d$ as defined in Eq. (14) and the exponents are $a=0.06$, $b=0.18$, $c=0.08$ and $d=2.26$.

4. Application

By applying Eq. (14) to the present segmented wheel/fluid chamber system shown in Figs. 1 and 3, the relationship below is obtained

$$Q_m^* = 4.5\times 10^3 (Re^*)^{0.06}(We^*)^{0.18}(\Delta p^*)^{0.08}(\phi^*)^{2.26} \quad (23)$$

where coefficient C_c and exponents a, b, c and d are determined using the method of multi-variable regression.

Fig. 8 shows that the model presents very well the experimental measurements with the mist flow rate ratio varying from 30% to 85%. The prediction shows that at a given wheel speed, an increase in coolant viscosity (thus smaller Reynolds number) will reduce the mist rate by a power factor of $a=0.06$. This effect, however, is smaller than that of the surface tension, as indicated by the higher exponent on the Weber number ($b=0.18$).

The positive exponent of $c=0.08$ indicates a slight influence of pressure drop on the increment of mist rate. It is more understandable if Eq. (7) is recalled. Since Δp varies with Q^2, the detrimental effect of pressure drop in raising the mist rate is trivial at small Q which is often the case with the current grinding system.

Eq. (23) stated that due to the slippage of the major coolant flow, it is necessary to align the fluid chamber inclined with the axis perpendicular to the surface subjected to grinding, i.e. with an angle ϕ. The introduction of ϕ can effectively reduce the mist flow rate, because the exponent on $\phi*$ is high ($d=2.26$).

The model demonstrates that the wheel speed ω has the most comprehensive influence on the mist formation because it appears in the majority of the dimensionless

Table 1
Experimental parameters

Grinding machine	Minini Junior 90 CNC-M286
Grinding wheel	Radius, $R=150$ mm
	144 segments
	Perforated hole diameter, $d_n=2$ mm
	Hole length $(z_1-z_2)=5$ mm
Fluid chamber	Material: Teflon (PTFE)
	Cross-sectional area, $A_1=88.3$ mm^2
	Number of perforated holes within the fluid chamber, $n=4$
Coolant, Noritake SA-02	Concentration: 1:60, 1:85
	Surface tension (N m^{-1}): $\approx 73.1\times 10^{-3}$ (water based)
	Dynamic viscosity (N s m^{-2}): 12.1×10^{-4}, 8.9×10^{-4}
	Density (kg m^{-3}): 980
	Flow rate (l min^{-1}): 4.3, 12.2, 18.8
Spindle speed (rpm)	100, 150, 375, 500, 600, 750, 1000, 1200, 1500
Coolant chamber alignment angle, ϕ	0°, 30°, 15°

variable groups, i.e., in Re^*, We^*, and Δp^*. Since the influence of Δp^* is small as discussed above, the contribution of ω is mainly on the change of Re^* and We^* and a higher wheel speed will clearly bring about a more significant mist formation rate. In manufacturing practice, a high production rate often requires a high wheel speed in grinding, but at the same time, a low mist ratio is desirable in reducing the environmental and occupational hazards, which in turn demands a low wheel speed. The present model described by Eq. (23) indicates that the state of low mist formation rate with a high wheel speed can be realised by increasing the alignment of the coolant chamber (ϕ), the viscosity (μ) and surface tension (σ) of coolant. This gives a useful guideline for the selection of coolant properties in the process planning to be operated at a high wheel speed with a low mist rate.

5. Conclusion

A parametric model has been developed to present the contributions of fluid properties, grinding parameters, fluid chamber details and its alignment to the formation of mists when a segmented grinding wheel system is used. The model prediction is in good agreement with the experimental data. The model can also be used to guide the selection and use of coolant in achieving a balanced consideration of productivity and environmental consciousness.

Acknowledgements

This work was supported by the Australia Research Council (ARC). The authors appreciate very much Mr. Y.L. Pai and Mr. J. Huang at Kink Grinding Wheel Corp. for making the wheel segments.

References

[1] A.S. Lavine, A simple model for convective heat transfer during the grinding process, Journal of Engineering for Industry 110 (1988) 1–6.

[2] D.D. Bell, J. Chou, S. Liang, Modeling of the environmental effect of cutting fluid, Tribology Transactions 42 (1) (1999) 168–173.

[3] T. Suto, T. Waida, H. Naguchi, H. Inoue, High performance creep feed grinding of difficult-to-machine materials, Bulletin of the Japan Society of Precision Engineering 24 (1) (1990) 39–44.

[4] L.C. Zhang, T. Nguyen, B. Oliver, A grinding wheel assembly and a method of grinding, Australia Patent No. 20044901614.

[5] L. Bayvel, Orzechowski, Liquid atomization, Combustion—An International series, Taylor and Francis, 1993.

[6] A.H. Lefebvre, Atomization and SPRAY, COMBUSTION—An International Series, Hemisphere Pub. Corp, 1989.

[7] S. Matsumoto, Y. Takashima, Atomization characteristics of power law fluids by rotating disks, First International Conference on Liquid Atomization and Spray Systems, Tokyo, Japan, 1978, pp. 145–150.

[8] R.P. Grant, S. Middleman, Newtonian jet stability, Journal for the American Institute of Chemical Engineers 12 (4) (1966) 669–678.

[9] Y. Kitamura, T. Takahashi, Stability of a liquid jet in air flow normal to the jet axis, Journal of Chemical Engineering, Japan 9 (4) (1976) 282–286.

[10] N. Dombrowski, W.R. Johns, The aerodynamic instability and disintegration of viscous sheets, Chemical Engineering Science 18 (1963) 203–214.

[11] N.A. Fleck, K.L. Johnson, M. Mear, L.C. Zhang, Cold rolling of thin foil, Journal of Engineering Manufacture, IMechE B206 (1992) 119–131.

[12] L.C. Zhang, On the mechanism of cold rolling thin foil, International Journal of Machine Tools and Manufacture 35 (1995) 363–372.

[13] J. Sun, L.C. Zhang, Y.-W. Mai, S. Payor, M. Hogg, Material removal in the optical polishing of hydrophilic polymer, Journal of Materials Processing Technology 103 (2000) 230–236.

[14] L.C. Zhang, T. Suto, H. Noguchi, T. Waida, Applied mechanics in grinding, part III: a new formula for contact length prediction and a comparison of available models, International Journal of Machine Tools and Manufacture 33 (4) (1993) 587–597.

[15] L.C. Zhang, T. Suto, H. Noguchi, T. Waida, Applied mechanics in grinding, Part II: modelling of elastic modulus of wheels and interface forces, International Journal of Machine Tools and Manufacture 33 (1993) 245–255.

[16] G. Lu, L.C. Zhang, Further remarks on the modelling of elastic modulus of grinding wheels, International Journal of Machine Tools and Manufacture 34 (1994) 841–846.

[17] T.X. Yu, L.C. Zhang, Plastic Bending: Theory and Applications, World Scientific, Singapore, 1996.

[18] M.J. McCarthy, Molloy, review of stability of liquid jets and the influence of nozzle design, The Chemical Engineering Journal 7 (1) (1974) 1–20.

[19] E. van de Sande, J.M. Smith, Jet breakup and air entrainment by low velocity turbulent jets, Chemical Engineering Science 31 (3) (1976) 219–224.